

Electronic Supplementary Information for

Influence of external magnetic field and magnetic-site dilution to the magnetic dynamics of one-dimensional Tb(III)-radical complex

Leilei Li, Shuang Liu, Han Li, Wei Shi* and Peng Cheng*

Department of Chemistry, Key Laboratory of Advanced Energy Materials Chemistry (MOE), and Collaborative Innovation Center of Chemical Science and Engineering (Tianjin), Nankai University, Tianjin 300071, P. R. China. Fax: +86-22-23502458; shiwei@nankai.edu.cn.

Table of Contents

Section S1	Materials and Methods	2
Section S2	Crystallographic Data	3
Section S3	Powder X-ray Diffraction (PXRD)	4
Section S4	3D Packing Structure of 1	5
Section S5	Other Magnetic Data	6-15
Section S6	Tables of Crystal Data and Magnetic Data	16-18
Section S7	References	19

1. Synthesis

Materials and General Characterization. All chemicals and solvents are reagent-grade and the n-heptane and dichloromethane were used after dried by Na and CaH₂, respectively. The radical NITPhCOOMe was synthesized with Methyl 4-formylbenzoate and 2,3-bis(hydroxylamino)-2,3-dimethylbutane by Ullman's procedure.¹ Ln(hfac)₃·2H₂O was prepared according to the literature method.² Elemental analyses for C, H and N were carried out on a Perkin–Elmer analyzer. Powder X-ray diffraction measurements were recorded on a D/Max-2500 X-ray diffractometer using Cu-K α radiation. Magnetic susceptibility measurements were performed on a Quantum Design SQUID VSM magnetometer. Diamagnetic corrections were made for all the constituent atoms with Pascal's constants and the sample holders. The ICP-AES measurements were performed on a USA Thermo Jarrell-Ash Corp ICP-9000(N+M) instrument.

Synthesis of [Tb(hfac)₃(NITPhCOOMe)]_n (**1**). A suspension of 0.04 mmol Ln(hfac)₃·2H₂O in 30.0 mL dry n-heptane was heated to reflux for 2 hours and then cooled to 70.0 °C, after that 0.04 mmol NITPhCOOMe in 5.0 mL dichloromethane was added under stirring. The mixture was stirred for another 5 minutes, and then cooled to room temperature. Slowly evaporation of the final solution for about one week yielded dark-blue block crystals suitable for single-crystal X-ray analysis. Yield (based on Ln): 30.7% for **1**, 35.2%. Elemental analysis calcd (%) for **1** (C₃₀H₂₂F₁₈TbN₂O₁₀): C, 33.63; H, 2.07; N, 2.61. Found: C, 33.84; H, 2.02; N, 3.01.

Syntheses of diluted samples. The diluted samples were obtained with the same procedure with complex **1** except that the Tb(hfac)₃·2H₂O was substituted with the mixture of Tb(hfac)₃·2H₂O and Y(hfac)₃·2H₂O with the ratio of 1:10 and 1:20. Elemental analysis calcd (%) for 1:10 sample (C₃₀H₂₂F₁₈Tb_{0.091}Y_{0.909}N₂O₁₀): C, 35.76; H, 2.20; N, 2.78. Found: C, 35.86; H, 2.52; N, 3.01. Elemental analysis calcd (%) for 1:20 sample (C₃₀H₂₂F₁₈Tb_{0.048}Y_{0.952}N₂O₁₀): C, 35.86; H, 2.21; N, 2.79. Found: C, 35.92; H, 2.10; N, 2.85.

2 Crystallographic Studies

Single-crystal X-ray diffraction measurement of **1** was recorded on an Oxford Supernova diffractometer with a graphite monochromatic $Mo-K\alpha$ radiation ($\lambda = 0.71073 \text{ \AA}$). The structure was solved by direct method and refined by full-matrix least-squares techniques on F^2 using the *SHELXS-97* and *SHELXS-97* programs.³ Anisotropic thermal parameters were assigned to all non-hydrogen atoms. The hydrogen atoms were placed in idealized positions and located in the difference Fourier map. The crystallographic data are listed in Table S1. CCDC 1044640 for **1** contains the supplementary crystallographic data for this paper. The data can be obtained free of charge from the Cambridge Crystallographic Data Centre (www.ccdc.cam.ac.uk/data_request/cif).

compound	1
formula	$C_{30}H_{22}N_2O_{10}F_{18}Tb$
formula weight	1071.42
crystal system	monoclinic
space group	$P2_1/c$
a (Å)	11.7995(1)
b (Å)	15.2788(2)
c (Å)	24.2493(3)
α (°)	90
β (°)	116.8680(3)
γ (°)	90
$V(\text{\AA}^3)$	3899.77(10)
Z	4
D_c , (g cm ⁻³)	1.825
μ , (mm ⁻¹)	1.789
F (000)	2092
GOF on F^2	1.027
R_{int}	0.0288
R_I , wR_2 [$I > \sigma(I)$]	0.0276, 0.0595
R_I , wR_2 (all data)	0.0337, 0.0628
Residues (e Å ⁻³)	0.984/-0.680

3 Power X-ray diffraction

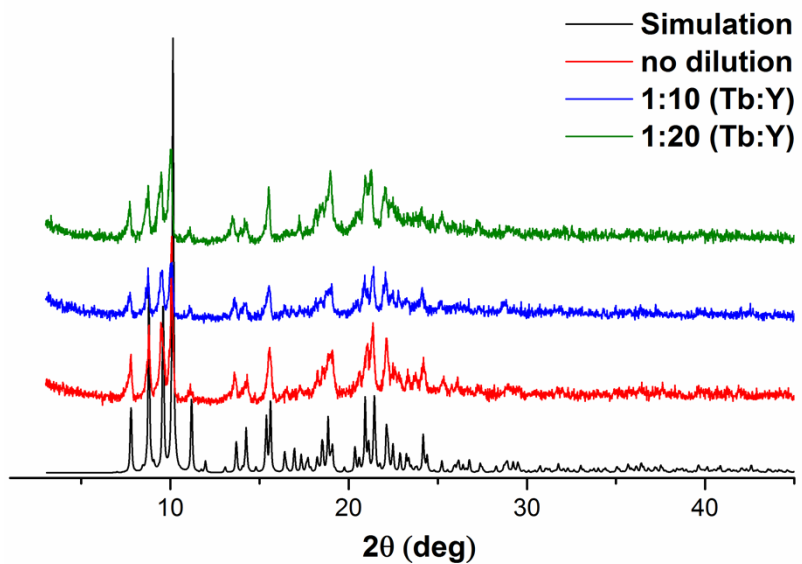


Fig. S1 Comparison of the experimental PXRD pattern of the as-synthesized **1** (no dilution) and diluted samples with the one simulated from its single crystal data.

4 Other crystal structure graphic

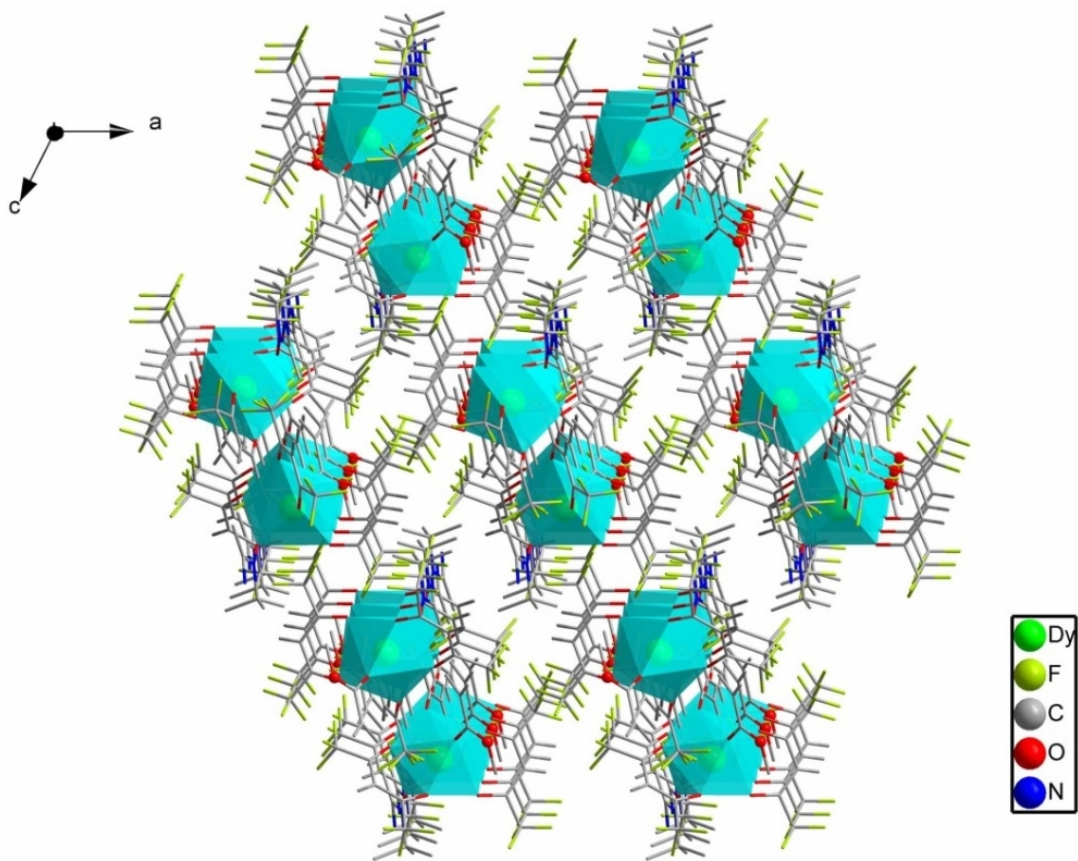


Fig. S2. Viewing of the 3D packing structure of **1**.

5 Other magnetic data

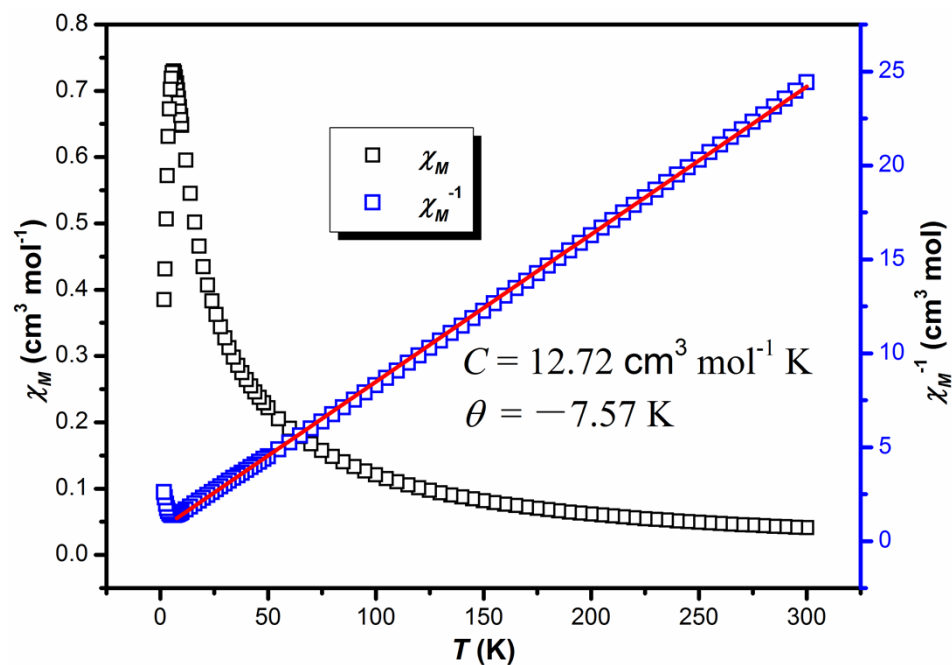


Fig. S3 Plot of χ_M vs. T and χ_M^{-1} vs. T of **1**. The red line represents the fitting result by Curie-Weiss law.

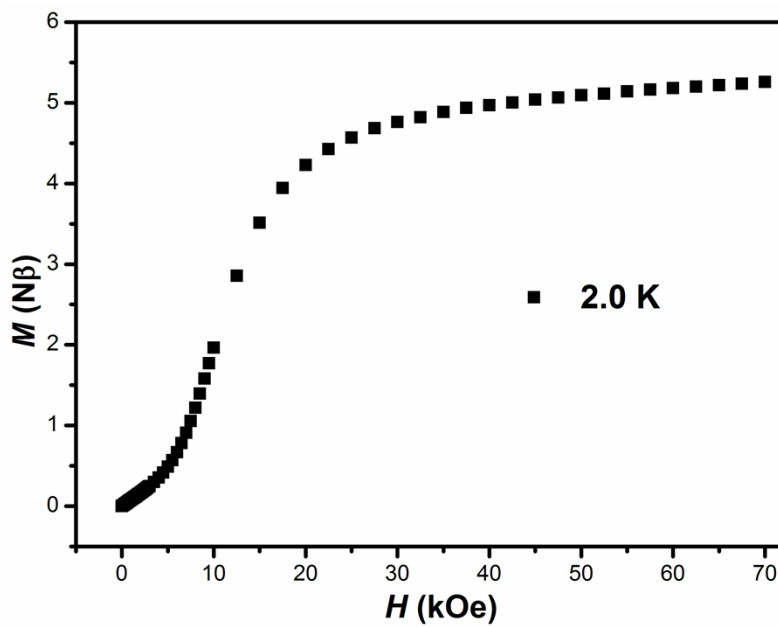


Fig. S4 Field dependence of magnetization of **1** at 2.0 K.

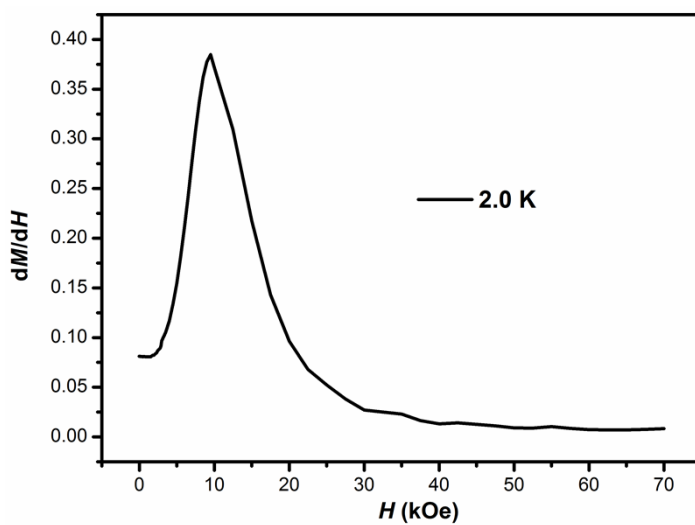


Fig. S5 Plot of dM/dH vs. H of **1** under 2.0 K.

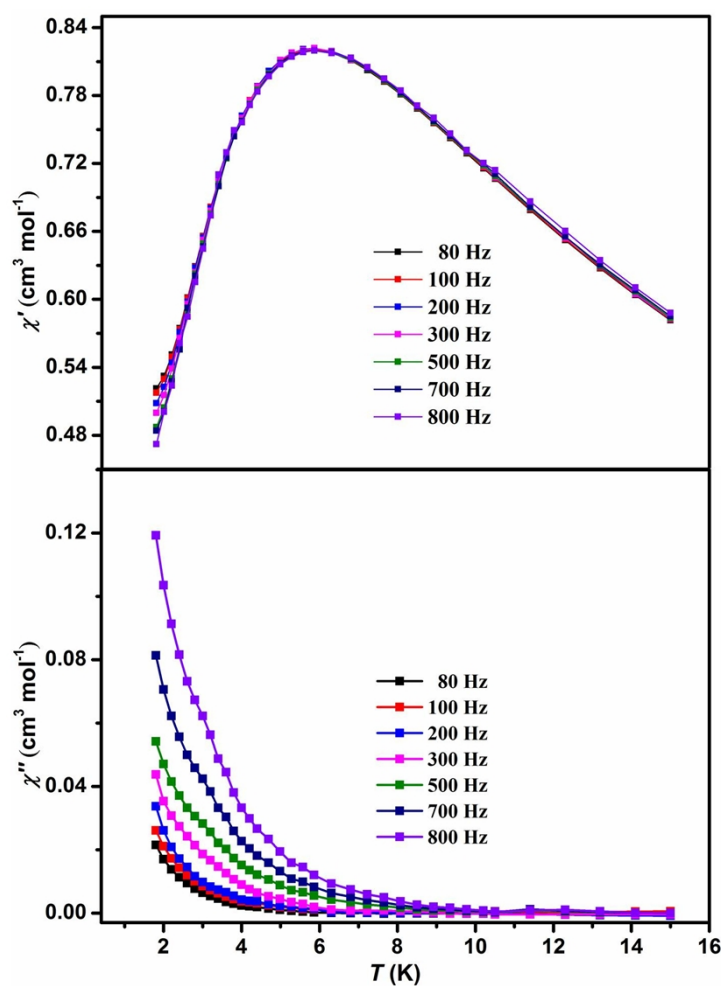


Fig. S6 The real (left) and imaginary (right) components of temperature dependence of ac magnetic susceptibility for **1** under zero applied dc field.

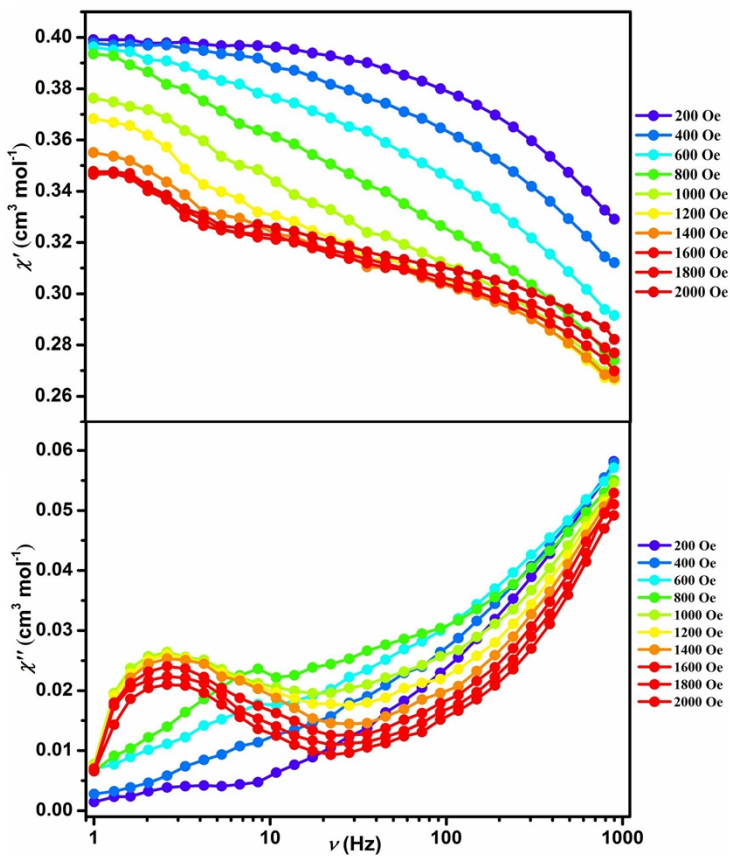


Fig. S7 The real (up) and imaginary (down) components of frequency dependence of ac magnetic susceptibility for **1** under varying applied dc fields at 1.8 K.

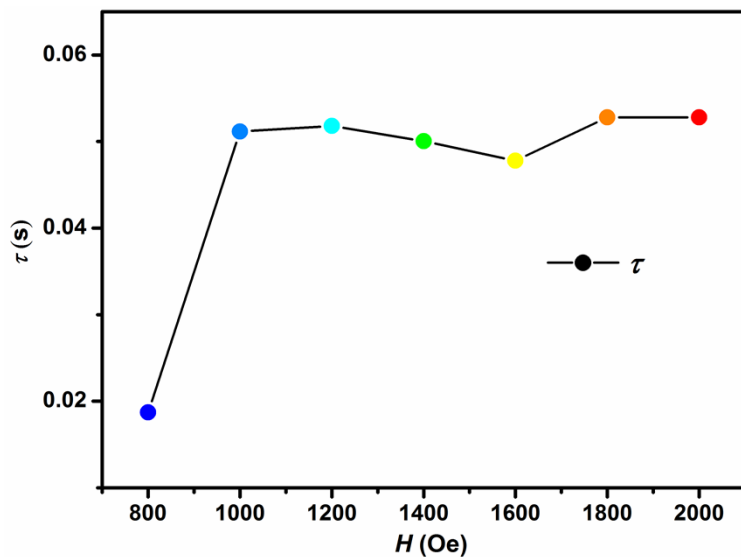


Fig. S8 Plot of τ vs. H for **1** under different dc fields at 1.8 K. The solid line is guide for eyes.

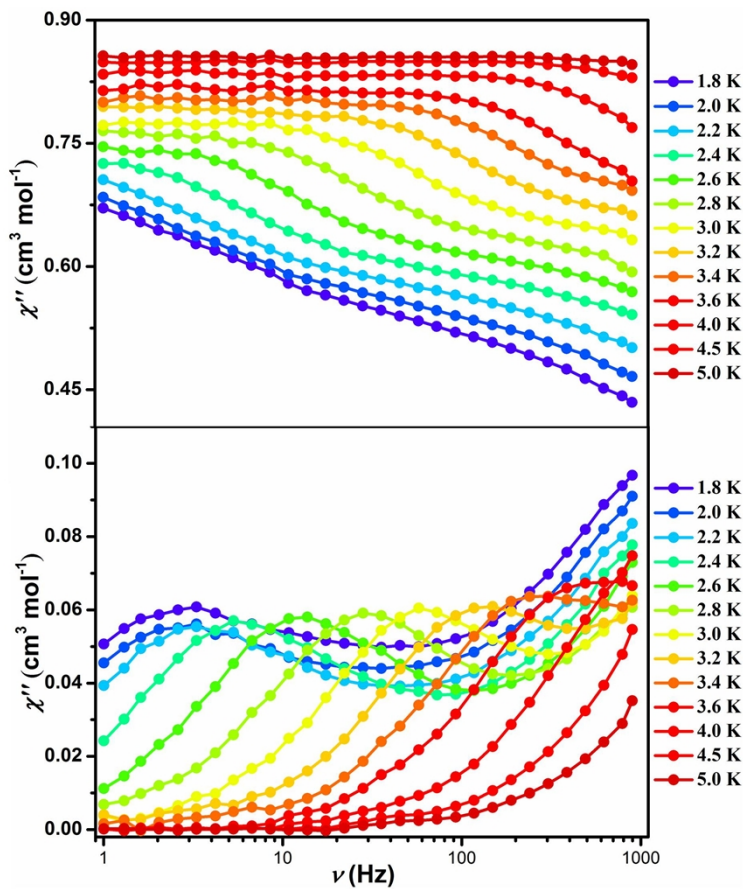


Fig. S9 The real and imaginary components of frequency dependence of ac magnetic susceptibility for **1** under 1000 Oe dc fields.

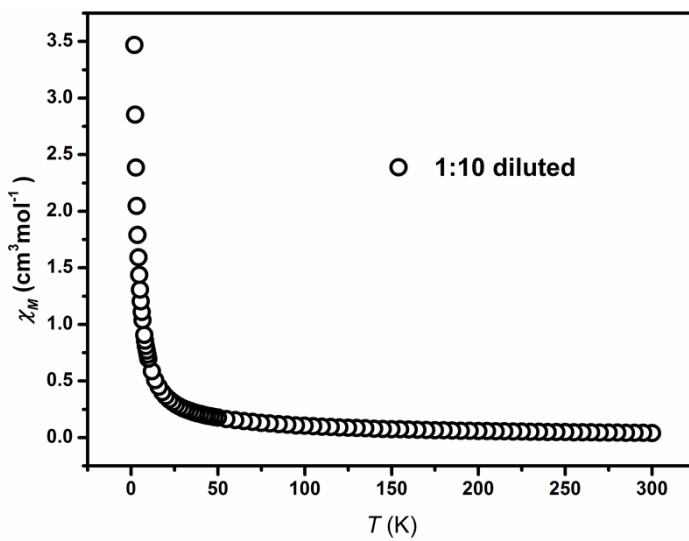


Fig. S10 Temperature dependence of dc magnetic susceptibility of 1:10 diluted sample under 1.0 kOe.

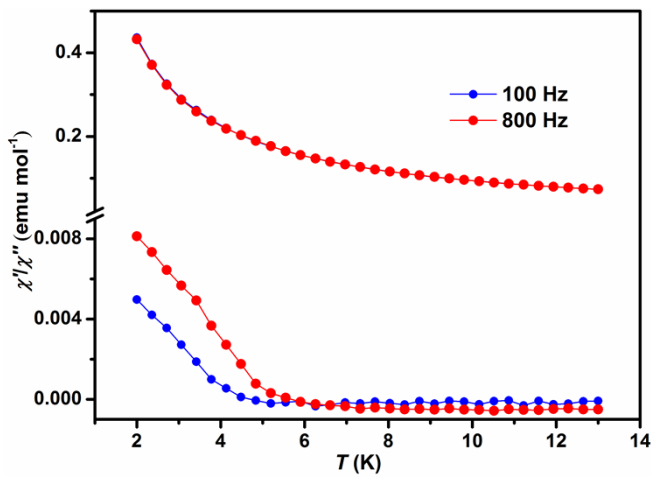


Fig. S11 Temperature dependence of ac susceptibility of 1:10 diluted sample under zero dc field.

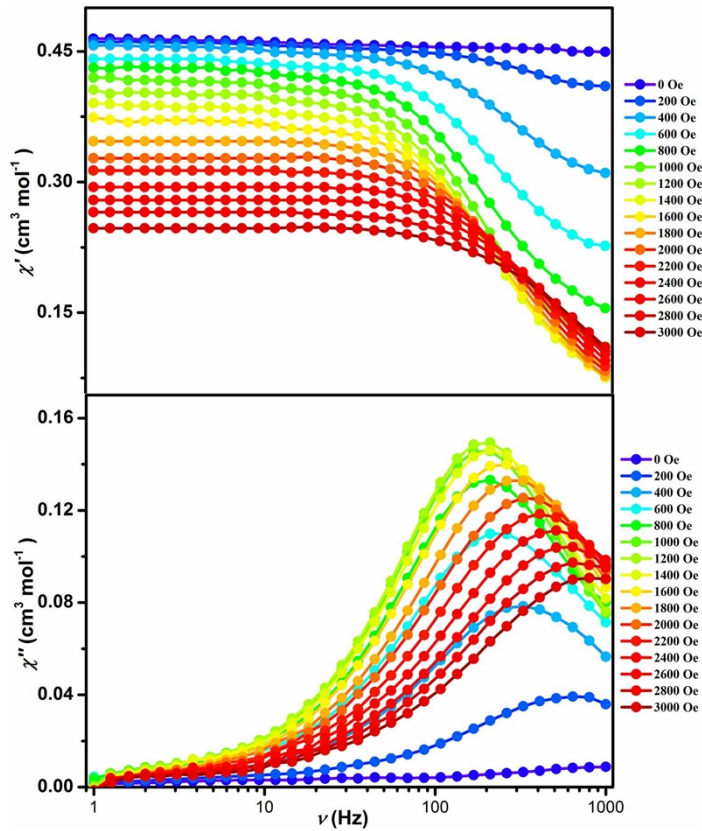


Fig. S12 The real (up) and imaginary (down) components of frequency dependence of ac magnetic susceptibility for **1:10** sample under different dc fields at 1.8 K.

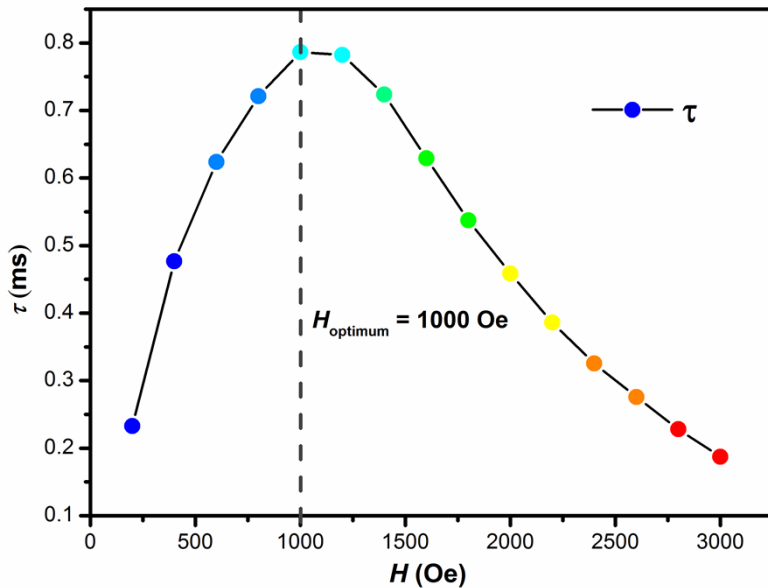


Fig. S13 Plot of τ vs. H for **1:10** sample under different dc fields at 1.8 K. The solid line The solid line represents the sum of tunneling process and direct process.

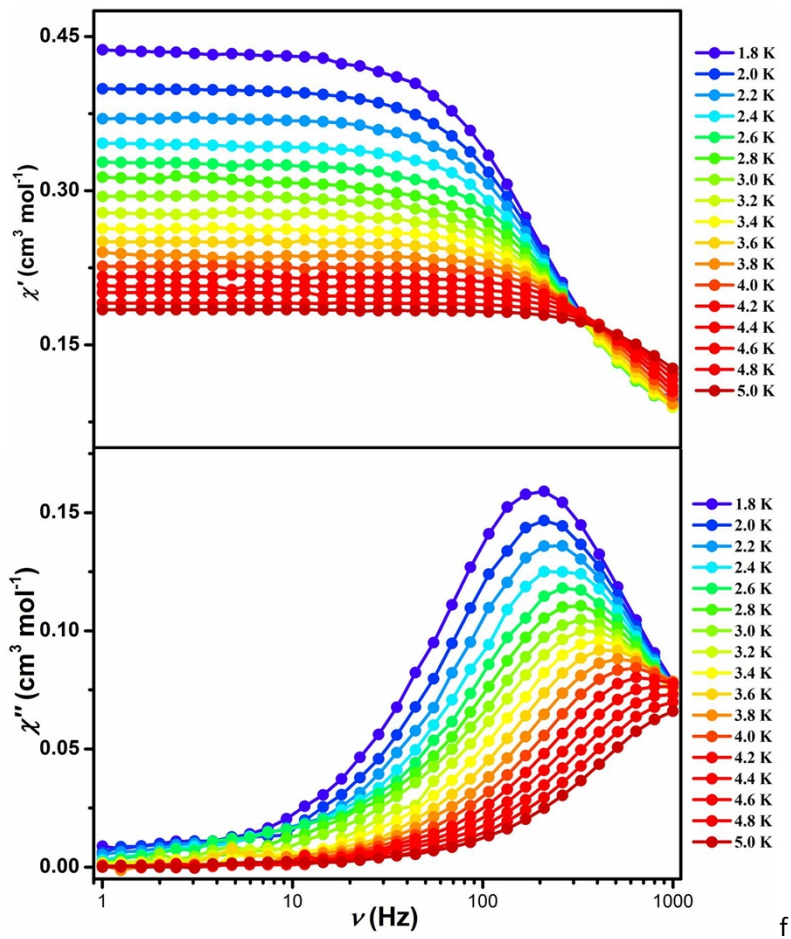
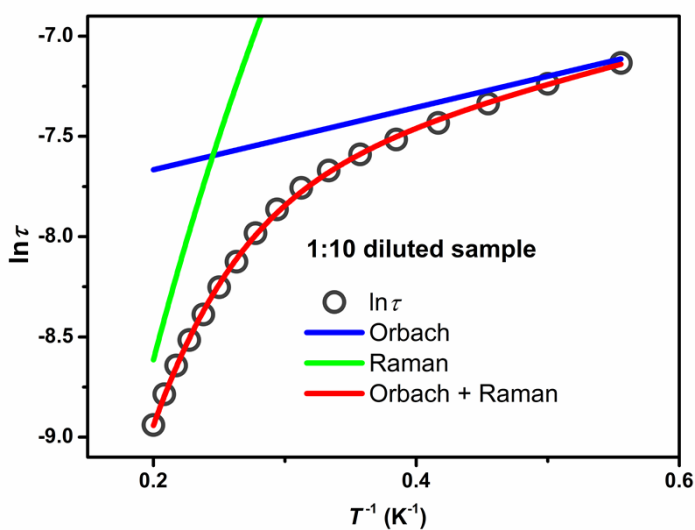
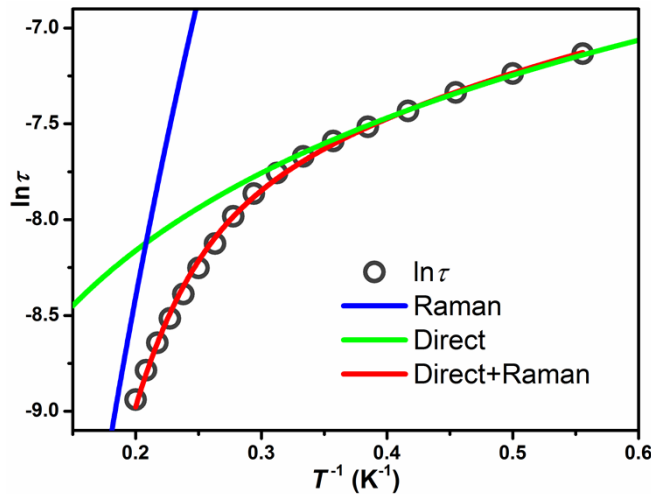
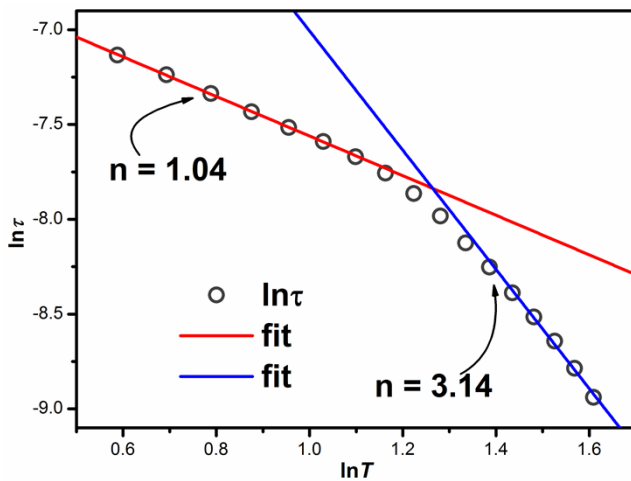


Fig. S14 The real component of frequency dependence of ac magnetic susceptibility for **1:10** sample under 1000 Oe dc field.



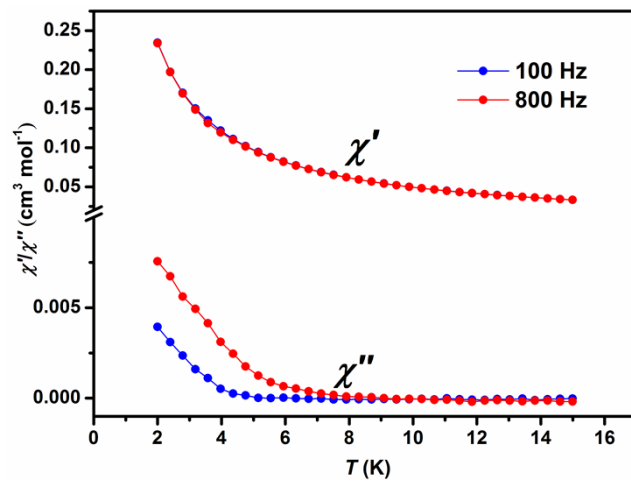


Fig. S18 Temperature dependence of ac susceptibility of 1:20 diluted sample under zero dc field

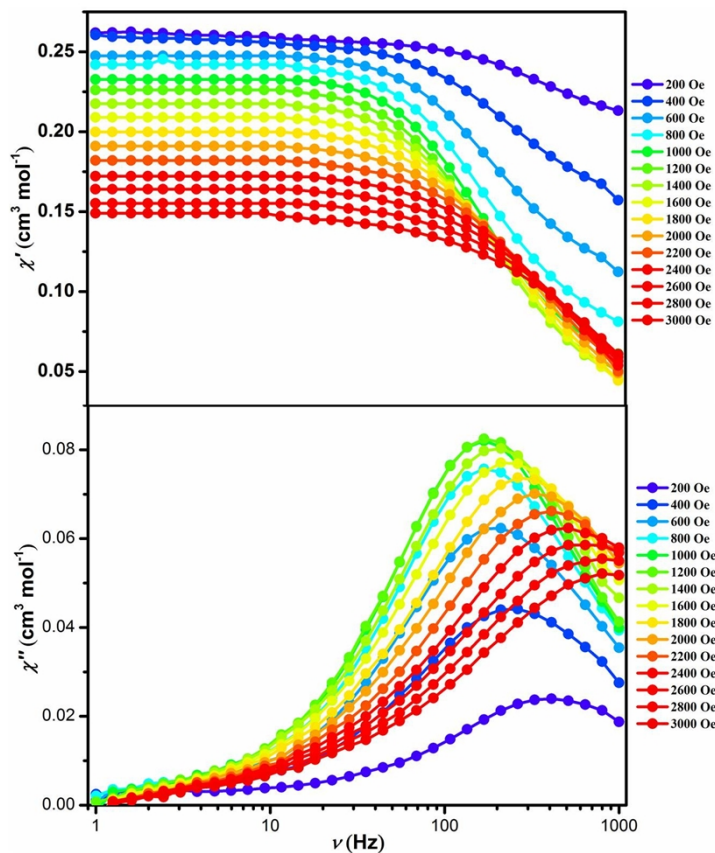


Fig. S19 The real (up) and imaginary (down) components of frequency dependence of ac magnetic susceptibility for **1:20** sample under different dc fields at 1.8 K.

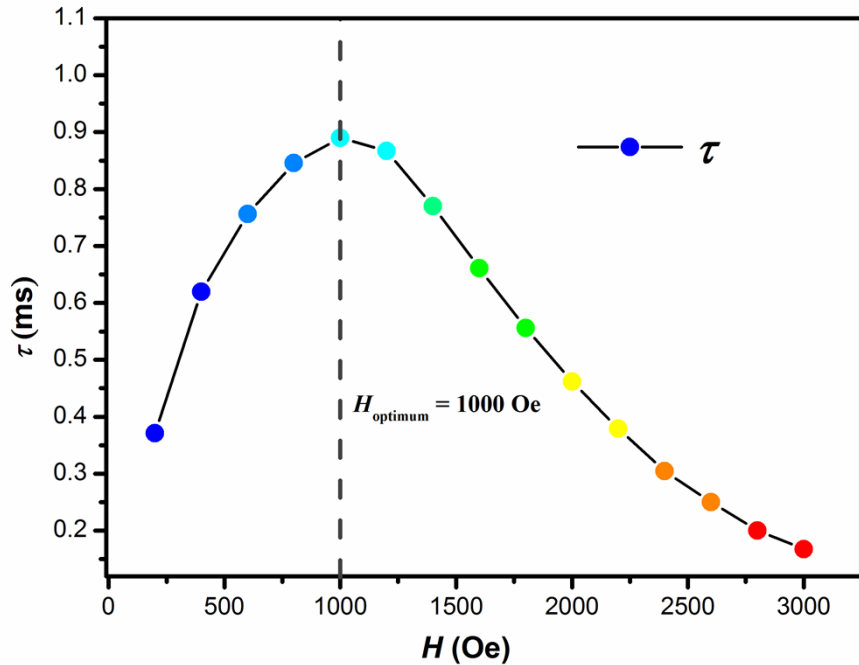


Fig. S20 Plot of τ vs. H for **1:20** sample under different dc fields at 1.8 K. The solid line represents the fitting using the sum of tunneling process and direct process.

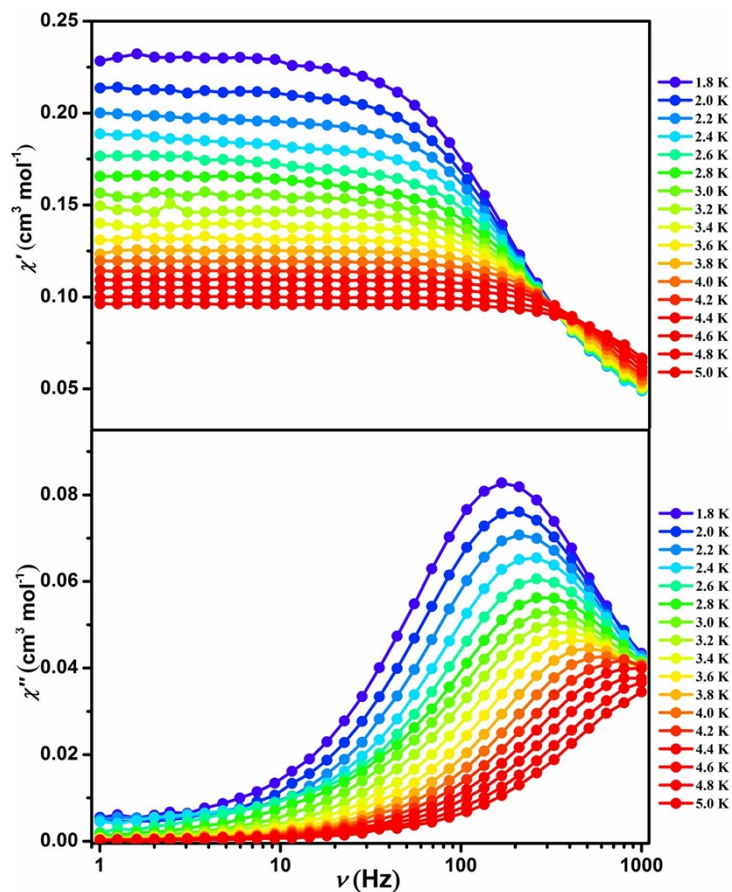


Fig. S21 The real component of frequency dependence of ac magnetic susceptibility for **1:20** sample under 1000 Oe dc fields.

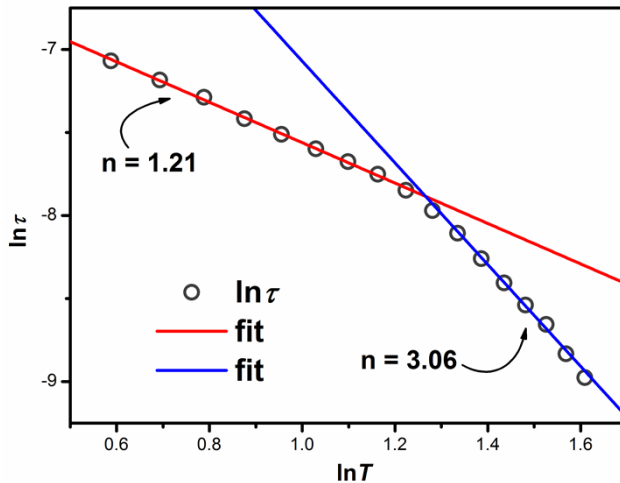


Fig. S22 Plot of $\ln\tau$ versus $\ln T$ for **1:20** diluted sample under 1000 Oe dc field. The solid line is linear fitting result.

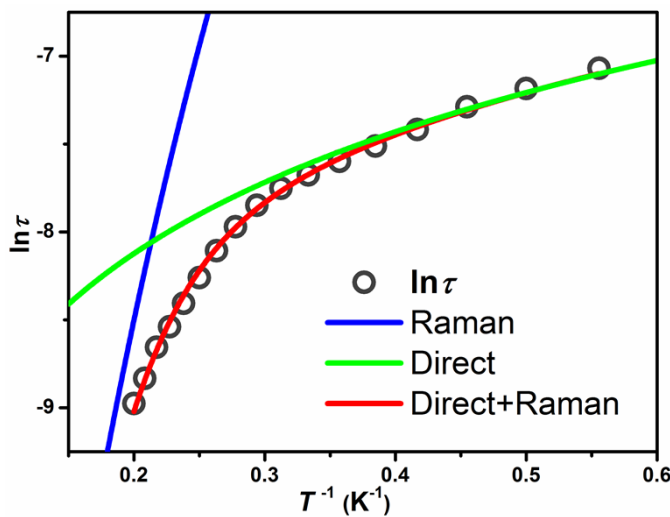


Fig. S23 Fitting result of $\ln\tau$ vs. T^{-1} plot using the mixture of Ram an plus direct process under 1000 Oe dc field.

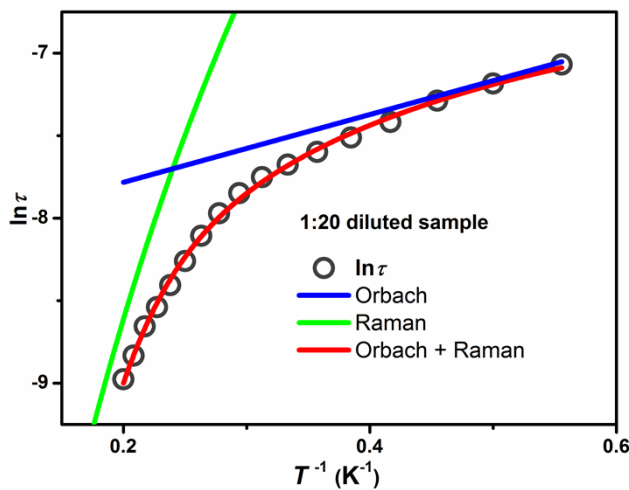


Fig. S24 Fitting result of $\ln\tau$ vs. T^{-1} plot using the mixture of Orbach plus Raman process under 1000 Oe dc field.

Table S1. Selected bond lengths and angles of complex **1**.

Bonds/Angles	1 (Å / °)
Tb(1)-O(5)	2.336(2)
Tb(1)-O(8)	2.336(2)
Tb(1)-O(7)	2.351(2)
Tb(1)-O(4)	2.356(2)
Tb(1)-O(1)	2.357(2)
Tb(1)-O(3)	2.368(2)
Tb(1)-O(9)	2.373(2)
Tb(1)-O(6)	2.401(2)
O(5)-Tb(1)-O(8)	80.55(7)
O(5)-Tb(1)-O(7)	140.65(8)
O(8)-Tb(1)-O(7)	73.81(7)
O(5)-Tb(1)-O(4)	149.40(7)
O(8)-Tb(1)-O(4)	115.67(8)
O(7)-Tb(1)-O(4)	69.88(7)
O(5)-Tb(1)-O(1)	89.34(7)
O(8)-Tb(1)-O(1)	75.60(7)
O(7)-Tb(1)-O(1)	111.91(7)
O(4)-Tb(1)-O(1)	71.52(7)
O(5)-Tb(1)-O(3)	78.80(7)
O(8)-Tb(1)-O(3)	143.31(7)
O(7)-Tb(1)-O(3)	137.57(7)
O(4)-Tb(1)-O(3)	73.19(7)
O(1)-Tb(1)-O(3)	74.18(7)
O(5)-Tb(1)-O(9)	96.74(8)
O(8)-Tb(1)-O(9)	140.73(7)
O(7)-Tb(1)-O(9)	85.33(7)
O(4)-Tb(1)-O(9)	86.25(8)
O(1)-Tb(1)-O(9)	143.67(8)
O(3)-Tb(1)-O(9)	72.00(7)
O(5)-Tb(1)-O(6)	71.76(8)
O(8)-Tb(1)-O(6)	72.71(8)
O(7)-Tb(1)-O(6)	72.38(8)
O(4)-Tb(1)-O(6)	136.28(7)
O(1)-Tb(1)-O(6)	145.21(8)
O(3)-Tb(1)-O(6)	127.31(8)
O(9)-Tb(1)-O(6)	69.36(8)

Table S2. δ' and ϕ values for TbO_8 geometry of **1**.

parameter	1(experiment)	Value (°)	Ideal	Model-	Ideal	Model-	Ideal	Model-
			D_{2d} (°)	C_{2v} (°)	D_{4d} (°)	D_{4d} (°)		
δ'	$\text{O}_4 [\text{O}_1 \text{O}_7] \text{O}_8$	3.816(89)	29.5		0.0		0.0	
	$\text{O}_3 [\text{O}_5 \text{O}_9] \text{O}_6$	26.872(91)	29.5		21.8		0.0	
	$\text{O}_3 [\text{O}_1 \text{O}_5] \text{O}_8$	45.727(68)	29.5		48.2		52.4	
	$\text{O}_4 [\text{O}_7 \text{O}_9] \text{O}_6$	43.268(81)	29.5		48.2		52.4	
ϕ	$\text{O}_1\text{-}\text{O}_9\text{-}\text{O}_8\text{-}\text{O}_6$	12.449(59)	0		14.1		24.5	
	$\text{O}_7\text{-}\text{O}_5\text{-}\text{O}_3\text{-}\text{O}_4$	17.389(57)	0		14.1		24.5	

Table S3. The best fitting parameters for the Arrhenius plots of complex **1** and diluted samples.

Compound	$\tau_{\text{QTM}}^{\text{a}}$ (s)	A ($\text{s}^{-1} \cdot \text{K}^{-1}$)	C ($\text{s}^{-1} \cdot \text{K}^{-m}$)	m	U_{eff} (K^{-1})	τ_0 (s)
1 (pure Tb, SR)	—	—	—	—	36(1)	$9.2(2) \times 10^{-7}$
1 (pure Tb, SR)	0.059(3)	—	—	—	36(1)	$2.0(3) \times 10^{-8}$
1:10 (Direct+Raman)	—	690(3)	0.057(2)	7	—	—
1:10 (Orbach+Direct)	—	692(4)	—	—	28(1)	$8(1) \times 10^{-7}$
1:10 (Orbach+Raman)	—	—	1.76(2)	5	1.55(7)	$3.4(1) \times 10^{-4}$
1:20 (Direct+Raman)	—	670(6)	0.063(2)	7	—	—
1:20 (Orbach+Direct)	—	672(6)	—	—	28(1)	$8(2) \times 10^{-7}$
1:20 (Orbach+Raman)	—	—	1.83(4)	5	2.1(2)	$3.0(2) \times 10^{-4}$

^aThe first row is the result fitting by Arrhenius law. The other rows represent the results fitting by equation $\tau^{-1} = \tau_{\text{QTM}}^{-1} + AT^n + CT^m + \tau_0^{-1} \exp(-U_{\text{eff}}/kT)$. The parameter n was fixed as 1 and m was fixed accordingly.⁴ The SR represents the slower relaxation process in **1**.

Table S4. The best fitting parameters for Cole-Cole plots of **1** at varying temperatures under 1000 Oe applied dc field using the sum of two modified Debye model.⁵

T (K)	$\chi_{\text{S,tot}}$	$\Delta\chi_1$	τ_1 (ms)	α_1	$\Delta\chi_2$	τ_2 (ms)	α_2
1.8	0.453989E-11	0.529259	0.0264219	0.397203	0.224813	58.8822	0.412958
2.0	0.886295E-11	0.549963	0.0207284	0.394550	0.197718	59.5193	0.393641
2.2	0.249214E-10	0.581351	0.0155888	0.409380	0.160186	47.0253	0.280620
2.4	0.256291E-10	0.600661	0.0133954	0.354451	0.141491	25.5482	0.183427
2.6	0.212421E-10	0.624851	0.0102057	0.355938	0.123707	12.7128	0.0924907
2.8	0.388899E-10	0.656278	0.00513318	0.441406	0.107791	6.38087	0.0540143
3.0	0.431114E-10	0.661809	0.00861083	0.237429	0.113580	2.91488	0.0552310
3.2	0.503568E-10	0.667632	0.00942338	0.0849461	0.124447	0.140002	0.0993379
3.4	0.696667E-10	0.687301	0.0101070	0.00104007	0.116491	0.799525	0.0631382
3.6	0.103298E-09	0.671078	0.00349239	0.00118561	0.145752	0.358725	0.0105512
4.0	0.185761E-09	0.670437	0.000219514	0.00547469	0.164413	0.137796	0.0594937
4.5	0.353996E-09	0.660664	0.000315778	0.00442307	0.189356	0.0532716	0.0507628
5.0	0.119523E-09	0.707363	0.000537849E-5	0.00903052	0.147926	0.0428146	0.00981016

Table S5. The best fitting parameters for Cole-Cole plots of **1:10** diluted sample at varying temperatures under 1000 Oe applied dc field.

T (K)	χ_T	χ_S	τ (ms)	α
1.8	0.0674953	0.434897	0.798187	0.0915729
2.0	0.0634803	0.399410	0.718832	0.0884892
2.2	0.0589891	0.371807	0.651746	0.0907762
2.4	0.0555555	0.345850	0.591539	0.0910207
2.6	0.0511848	0.327829	0.544645	0.106126
2.8	0.0483661	0.312619	0.505373	0.116258
3.0	0.0482219	0.295029	0.466460	0.107119
3.2	0.0502533	0.278671	0.428143	0.0819636
3.4	0.0502263	0.262731	0.384307	0.0636999
3.6	0.0493820	0.250515	0.341378	0.0532485
3.8	0.0465524	0.237326	0.296213	0.0420521
4.0	0.0469655	0.226376	0.260740	0.0353487
4.2	0.0455616	0.216548	0.227499	0.0348066
4.4	0.0452455	0.207267	0.200470	0.0304035
4.6	0.0456235	0.198917	0.176327	0.0286245
4.8	0.0443711	0.191329	0.152780	0.0290668
5.0	0.0422393	0.184086	0.131190	0.0291655

Table S6. The best fitting parameters for Cole-Cole plots of **1:20** diluted sample at varying temperatures under 1000 Oe applied dc field.

T (K)	χ_T	χ_S	τ (ms)	α
1.8	0.032898	0.232121	0.851498	0.121287
2.0	0.0307937	0.213939	0.759117	0.118465
2.2	0.0299013	0.198865	0.683727	0.115617
2.4	0.0259339	0.186432	0.601041	0.132422
2.6	0.0251773	0.175752	0.54684	0.145881
2.8	0.0245031	0.166035	0.501246	0.147258
3.0	0.0257946	0.156384	0.464180	0.129202
3.2	0.0272530	0.147941	0.430224	0.110277
3.4	0.0280908	0.139648	0.390173	0.0855779
3.6	0.0280096	0.132211	0.345692	0.0672208
3.8	0.0272208	0.125607	0.301435	0.0570878
4.0	0.0253931	0.119838	0.258646	0.0555202
4.2	0.0238531	0.114380	0.223689	0.0506693
4.4	0.0234513	0.109512	0.195740	0.0450827
4.6	0.0243265	0.105016	0.174130	0.0377548
4.8	0.0216424	0.100088	0.145767	0.0417930
5.0	0.0210595	0.0962060	0.126305	0.0373844

6 References

- 1 E. F. Ullman, J. H. Osiecki, D. G. B. Boocock and R. Darcy, *J. Am. Chem. Soc.*, 1972, **94**, 7049.
- 2 K. Bernot, L. Bogani, A. Caneschi, D. Gatteschi and R. Sessoli. *J. Am. Chem. Soc.*, 2006, **128**, 7974.
- 3 G. Sheldrick, *Acta Crystallogr.*, 2008, **A64**, 112.
- 4 (a) K. R. Meihaus, S. G. Minasian, W. W. Lukens, Jr., S. A. Kozimor, D. K. Shuh, T. Tyliszczak and J. R. Long, *J. Am. Chem. Soc.*, 2014, **136**, 6065; (b) S. Demir, J. M. Zadrozny and J. R. Long, *Chem. Eur. J.*, 2014, **20**, 9524.
- 5 Y.-N. Guo, G.-X. Xu, W. Wernsdorfer, L. Ungur, Y. Guo, J. Tang, H.-J. Zhangg, L. F. Chibotaru and A. K. Powell, *J. Am. Chem. Soc.*, 2011, **133**, 11948.